ELSEVIER

Polymer 41 (2000) 3437–3453

polymer

Thermal behaviour and morphology of homogeneous ethylene–propylene and ethylene–1-butene copolymers with high comonomer contents

S. Vanden Eynde[a], V. Mathot[a,*], M.H.J. Koch[b], H. Reynaers[a]

[a]*Laboratorium voor Macromoleculaire Structuurchemie, Departement Scheikunde, Katholieke Universiteit Leuven, Celestijnenlaan 200F, B-3001 Heverlee, Belgium*

[b]*European Molecular Biology Laboratory, EMBL c/o DESY, Notkestraße 85, D-22603 Hamburg, Germany*

Received 7 June 1999; accepted 9 June 1999

Abstract

The thermal behaviour and morphology of series of homogeneous ethylene–propylene and ethylene–1-butene copolymers, which cover wide ranges in comonomer content, are studied by differential scanning calorimetry (DSC), time-resolved small-angle X-ray scattering (SAXS), wide-angle X-ray diffraction (WAXD) and transmission electron microscopy (TEM). The thermal behaviour and the morphology of the copolymers change in a continuous way as the comonomer content is increased, supporting the model in which the morphology changes gradually from a lamellar base morphology into a granular one consisting of small block-shaped structures. When the comonomer amount is raised further to very high contents, possibly via fringed-micelles a morphology consisting of loosely packed ethylene sequences is obtained. Although the granular structures, present in the very-low-density copolymers, are too small and/or too imperfect to be detected by WAXD, the crystallisation and melting processes could still be readily measured by DSC and SAXS.

Real-time SAXS measurements during a scan-iso temperature–time heating program, as used in some temperature-modulated DSC (TMDSC) measurements, shows that in a homogeneous ethylene–1-butene copolymer (6.4 mole% 1-butene) considerable instantaneous structural changes occur during dynamic (heating) and static (isothermal) measurements, as is, for instance, reflected in the significant increase of the SAXS invariant during the short isothermal stays.

Keywords: Crystallisation; Differential scanning calorimetry; Homogeneous ethylene–1-alkene copolymers

1. Introduction

Today, the polymers with the largest volume of sales on worldwide scale are polypropylene (PP) and polyethylene (PE) [1]. The term *polyethylene*, however, no longer refers to a single polymer, but covers a *class* of ethylene-based polymers with widely differing structures and properties [1–4]. Polyethylenes can be classified in linear polyethylene (LPE) and branched polyethylenes. The latter include high-density polyethylene (HDPE), low-density polyethylene (LDPE) and ethylene copolymers. HDPE contains less than one short side-chain per 200 carbon atoms in the main chain and has a relatively high crystallinity. In contrast, LDPE exhibits a considerable amount of both long- and short-chain branches. For ethylene copolymers the distinction has to be made between heterogeneous and homogeneous copolymers. The ethylene–propylene (EP) and ethylene–1-butene (EB) copolymers, investigated in the present study, are called *homogeneous copolymers* [1], because the way in which the comonomer is added during polymerisation can be described by a single set of chain propagation probabilities (P-set). All chains have the same comonomer/monomer ratio and statistically there are no differences within and between the molecules. In contrast to the linear-low-density and very-low-density polyethylenes (LLDPEs and VLDPEs, respectively) [1,5] which are *heterogeneous* with respect to the intermolecular distribution of the side-chain branches, the homogeneous copolymers investigated here have a relative narrow molar mass distribution and a constant comonomer content for all chains, while all chains have the same comonomer distribution. This homogeneity makes them very attractive for fundamental studies [2,3,6–8] and provides excellent prospects for an unambiguous interpretation of experimental data of short branched polyethylenes. Moreover, these materials are of increasing importance because of their recent commercialisation made possible by metallocene catalysis [9–11] and their potential applications, e.g. use as impact modifier, in food packaging, etc.

* Corresponding author.
E-mail address: vincent.mathot@chem.kuleuven.ac.be (V. Mathot).

0032-3861/00/$ - see front matter
PII: S0032-3861(99)00501-7

Table 1
Molecular characteristics of the LPE sample and the homogeneous ethylene–1-alkene compolymers

Sample	Comonomer content (mole%)	Catalyst[a]	$D^{23°C}$ (kg/m^3)[b]	M_n^* (kg/m^3)[b]	M_w^* (kg/mol)[b]	M_z^* (kg/mol)[b]
JW 1114 (LPE)	0.0	V	n.d	20	42	99
EP 208	$X_3 = 4.4$	V	923	41	91	160
EP 207	$X_3 = 10.6$	V	896	39	120	220
EP 203	$X_3 = 17.4$	V	n.d.	25	170	320
EP 201	$X_3 = 19.0$	V	n.d.	62	207	370
EP 243	$X_3 = 22.4$	V	n.d.	n.d.	n.d.	n.d.
EP 212	$X_3 = 24.7$	V	n.d.	41	91	160
EP 159	$X_3 = 26.4$	V	n.d.	78	184	320
EP 198	$X_3 = 30.8$	V	n.d.	105	270	470
EP 197	$X_3 = 35.3$	V	n.d.	78	190	350
EB 1	$X_4 = 4.0$	M	910	53	115	190
EB 2	$X_4 = 6.4$	M	901	54	115	180
EB 3	$X_4 = 10.7$	M	884	n.d.	n.d.	n.d.
EB 5	$X_4 = 12.0$	M	878	n.d.	n.d.	n.d.
EO V	$X_8 = 11.5$	V	872	110	215	350

[a] V = Vanadium based, M = Metallocene based.
[b] n.d. = Not determined.

In ethylene–1-alkene copolymers, each incorporation of a 1-alkene or α-olefin comonomer unit introduces a short-chain branch in the polymer chain causing a disruption of the chain regularity. The length of the side chain, which is controlled by the comonomer used, determines whether or not it will be incorporated in the crystalline regions. There is a broad consensus on the fact that methyl branches are incorporated at interstitial positions [12–14], which gives rise to crystal defects. In contrast, hexyl branches are completely rejected from the crystal lattice. Longer branches will not be incorporated either, but side-chain crystallisation of the branches might occur [15,16].

The structure of semi-crystalline polymers can be described as consisting of crystalline and amorphous phases. This separation into two phases with different electron densities makes the morphology of polyethylene and its copolymers very accessible to scattering techniques such as small-angle X-ray scattering (SAXS) and wide-angle X-ray diffraction (WAXD). From the morphological structural parameters and the invariant obtained from SAXS, conclusions can also be drawn as to the crystallisation and melting behaviour. Synchrotron radiation provides the opportunity to explore phase transitions, crystallisation, melting, annealing and mechanical performance in real time [17,18]. A profound analysis of the SAXS data of copolymers that reveal a lamellar morphology in TEM [2,3], using linear correlation functions [8], gives information about the long period, the crystalline lamellar thickness, the amorphous layer thickness and the crystallinity. For copolymers with higher comonomer contents no correlation functions were calculated because TEM on these samples reveals a granular base morphology consisting of small, imperfect block-shaped crystallites. The WAXD data were used to calculate crystallinities and to determine the crystal lattice. Identical temperature–time procedures were used in DSC and time-resolved SAXS/WAXD measurements to make full use of the complementarity of the two methods for the interpretation of the crystallisation and melting behaviour as well as the morphology of the samples.

2. Experimental

2.1. Samples

The homogeneous ethylene–propylene (EP) copolymers were synthesised by use of a homogeneous vanadium-based catalyst [6,8,19,20], while the homogeneous ethylene–1-butene (EB) copolymers were copolymerised using a metallocene catalyst. A linear polyethylene (LPE) sample, JW 1114, was also included as reference in this study. The comonomer content was tuned by varying the comonomer/ethylene ratio. The EP copolymer series covers a wide range of comonomer contents up to 35 mole% propylene. The EB copolymer series is limited to a comonomer amount of 12 mole% 1-butene. For each copolymer studied the comonomer inclusion is *homogeneous*. The molecular structure data and densities of the investigated ethylene–1-alkene copolymers are listed in Table 1. The (apparent) weight- and number molar masses were determined by size exclusion chromatography (SEC) in 1,2,4-trichlorobenzene at 135 or 150°C using universal (indicated by *) calibrations. The comonomer content was determined by ^{13}C-NMR. The densities at room temperature were obtained after compression moulding.

2.2. Techniques and methods

2.2.1. Differential scanning calorimetry

The DSC measurements were performed with a TA Instruments 2920 DSC in helium atmosphere. The cooling was provided by a pulsating nitrogen supply. The temperature calibrations were made using the melting onset

temperature of pure indium ($T_m^{onset} = 156.61°C$) and benzophenone ($T_m^{onset} = 48.00°C$). The sample masses varied from 5 to 20 mg with increasing comonomer content or decreasing density. The masses were weighed with an accuracy of 0.02 mg. After a waiting time of 5 min in the melt at 180°C to erase former history, the (co)polymer was cooled at −10°C/min to −90°C and, after 5 min, heated at the same rate. The contribution of an empty pan was subtracted from each measurement.

Because the determination of the peak maximum in the DSC curves was not always evident, especially in case of copolymers with high comonomer contents, characteristic crystallisation (T_c) and melting (T_m) temperatures of the copolymers were not only identified with the maximum in the exo- and endotherm respectively (T_x^{peak}), but also defined in two other ways: (1) the temperature at the cross-section of the extrapolation from the melt and the extrapolation from the peak shoulder at the high temperature side (T_x^{eo}, extrapolated on/offset) and (2) the temperature at which the DSC signal takes off from the extrapolation from the melt at the high temperature side (T_x^{ro}, real on/offset). The glass transition temperature (T_g) was calculated using the enthalpy method [21–23].

The mass fraction crystallinity as a function of temperature, $w^c(T)$, was calculated from the DSC curves after Mathot et al. [24,25], in which calculations the enthalpy measured, $h(T)$, is compared with the reference enthalpies for amorphous polyethylene, $h_a(T)$, and crystalline polyethylene, $h_c(T)$. A linear extrapolation from the melt was used as a good approximation of the heat flow of the fully amorphous phase [25]. The mass fraction crystallinity was calculated as a function of temperature using Eq. (1):

$$w^c(T) = \frac{(A_1 - A_2)_T}{h_a(T) - h_c(T)} \quad (1)$$

where A_1 and A_2 are the areas enclosed above and below the linear extrapolation from the melt, respectively, and the curve measured. Eq. (1) is based on Eq. (2), which results from the additivity of the enthalpies of the crystalline and amorphous phases.

$$w^c(T) = \frac{h_a(T) - h(T)}{h_a(T) - h_c(T)} \quad (2)$$

The reference values for linear polyethylene were taken from literature [26]. At temperatures above 17°C the values of the heat capacity of the amorphous phase, $c_{pa}(T)$, for LPE were used [26], which are based on Eq. (10) in Wunderlich and Czornyj [27]. Below this temperature, these $c_{pa}(T)$ values were extrapolated to the lowest temperatures by continuation of Eq. (10). A $c_{pa}(T)$ value deviating from that of LPE below 17°C was chosen because the copolymers discussed here have glass transitions around −50°C, of which the position and abruptness depend on the type and the amount of comonomer. With increasing comonomer content, the copolymers have increasingly sharper glass transitions. By contrast, LPE exhibits a gradual change in $c_{pa}(T)$ between about −153 and 17°C, which may be interpreted as a continuous glass transition extending over a very wide temperature range [26].

2.2.2. Time-resolved small-angle X-ray scattering/wide-angle X-ray diffraction

The time-resolved simultaneous SAXS/WAXD measurements were performed on the X33 double focusing camera of the EMBL in HASYLAB, at the storage ring DORIS III of the Deutsches Elektronen Synchrotron (DESY, Hamburg) using a wavelength of 1.5 Å [28]. The camera was equipped with a multiwire quadrant detector (SAXS) with delay line readout [29] located at 3.5 m from the sample position. The scattering vector, $s = 2 \sin \theta/\lambda$, where 2θ is the scattering angle and λ the wavelength, was calibrated using the first nine orders of dry calcified turkey tendon collagen, with a spacing of 640 Å. In the WAXD region, 2θ was calibrated using the 110- and 200-reflections of quenched JW 1114 (LPE) at 50°C, previously measured at the same temperature on a Rigaku high-temperature X-ray diffractometer which was calibrated with a silicon standard.

The SAXS/WAXD measurements were performed on samples of about 1 mm thickness. After a waiting time of 5 min in the melt, the sample was cooled at −1°C/min to room temperature (EB) or cooled at −10°C/min to −60°C (EP) and subsequently heated into the melt at 10°C/min using a Mettler FP-82HT hot stage, mounted perpendicularly to the incident X-ray beam. The hot stage was flushed with nitrogen to achieve controlled cooling to −60°C and was calibrated using the melting point of benzoic acid ($T_m = 122°C$).

SAXS measurements were also performed during a scan-iso temperature–time program, as is sometimes used in temperature-modulated DSC (TMDSC) experiments [30–32]. EB 2 samples, previously cooled at −1°C/min or quenched from the melt, were heated from 30 to 120°C at a rate of 2.5°C/min. Every 5°C or 2 min, an isothermal stay was introduced. This is equivalent to superimposing a constant heating rate and a saw-tooth modulation with a period of 4.5 min.

The SAXS and WAXD intensities were normalised to the intensity of the primary beam. The SAXS patterns were corrected for the detector response and an averaged melt pattern was subtracted from each diffraction pattern as a background correction.

The SAXS-invariant, $Q(T)$, or total scattering power of the system which is independent of the size and the shape of the scattering entities, was calculated by integration of the scattering intensity $I(s,T)$ with respect to s:

$$Q(T) = \int_0^\infty I(s,T)s^2 \, ds \quad (3)$$

In case of an ideal two-phase system the invariant is

described by

$$Q_{id}(T) = C\alpha_s\phi_L(T)[1 - \phi_L(T)][d_c(T) - d_a(T)]^2 \quad (4)$$

where the constant C depends on the instrument and represents the conversion factor from mass density (g/cm^3) to electron density (mol e$^-$/cm^3); α_s represents the fraction of semi-crystalline regions within the total irradiated sample volume [33]; $\phi_L(T)$ is the local volume fraction crystallinity in the semi-crystalline regions; $d_c(T)$ is the density of the crystalline phase and $d_a(T)$ the density of the amorphous phase. Note that in the calculation of the invariant according to Eq. (4) the temperature dependencies of the mass densities and the crystallinity are taken into account.

For the copolymer revealing a *lamellar morphology* in TEM, linear correlation functions were calculated and further analysed after Goderis et al. [8] in order to obtain information about morphological parameters such as the long period (LP), the crystalline lamellar thickness (L_c), the amorphous layer thickness (L_a) and ϕ_L. The SAXS curves were extrapolated to higher angles using a damped Porod function [34]. Because the linear correlation functions of the investigated samples did not reveal flat minima, the crystallinity was calculated using the quadratic expression [8]:

$$A = \phi_L(1 - \phi_L)\mathrm{LP} \quad (5)$$

with A is the intercept of the linear regression to the autocorrelation triangle with the ordinate. To compare crystallinities obtained by DSC and WAXD, which are *mass* crystallinities, with the *volume* crystallinities calculated from SAXS data, the latter were converted into mass crystallinities using Eq. (6) [35] and Swan's [36] temperature-dependent mass densities:

$$w^c(T) = \frac{d_c(T)}{d_c(T) + \left(\frac{1}{\phi(T)} - 1\right)d_a(T)} \quad (6)$$

The present method of interpretation of the SAXS curves, in terms of LP, L_a and L_c, gives meaningful results as long as the basic assumption, that the material consists of a lamellar morphology, is fulfilled. This is also the case if the lamellae occur isolated, which is actually the case for several of the present copolymers.

2.2.3. Static WAXD

The static wide-angle X-ray diffractograms at room temperature were obtained in the reflection mode using Ni-filtered Cu K_α-radiation from a Rigaku Rotaflex RU-200B rotating anode equipped with a horizontal Bragg–Brentano focussing diffractometer and a scintillation counter. The patterns were recorded in steps of $\Delta 2\theta = 0.05°$ in the range $3° \leq 2\theta \leq 60°$ with a measuring time of 3 s per step. The WAXD patterns were neither Lorentz-corrected nor corrected for polarisation, but a linear background was subtracted. The sample thickness was about 0.8 mm. Thermal treatments were either cooling at 10°C/min from the melt (in a Mettler hot stage) or quenching from the melt in a CO_2–isopropanol bath (−70°C). The multiple peak data were resolved into individual crystalline peaks and an amorphous halo using a peak fitting program for spectral data. Best fits were obtained using Pearson-peak profiles. The crystallinity index (χ_c) was calculated as the ratio of the total area under the resolved crystalline peaks (A_c) to the sum of the areas of the resolved crystalline peaks (A_c) and the amorphous halo (A_a):

$$\chi_c = \frac{A_c}{A_c + A_a} \quad (7)$$

The fraction crystallinity (index), when determined by Eq. (7), refers to the mass fraction of the total polymer which is sufficiently ordered to give an X-ray diffraction pattern characteristic of crystalline materials, rather than a diffuse halo [37].

2.2.4. Transmission electron microscopy [3]

Compression moulded sample plaques of 1 mm thickness and 5 mm in diameter were cooled from 150°C to room temperature at 10°C/min using DSC equipment. After further cooling to −120°C and trimming at that temperature, the samples were stained with chlorosulphonic acid vapour at room temperature to enhance the contrast between the crystalline and amorphous regions. The TEM studies were performed on sample coupes of approximately 100 nm thickness using a Philips CM 200TEM at 120 kV. One should bear in mind that most of the copolymers discussed here are not completely crystallised at room temperature. Therefore, the presented micrographs are only representative for the part of a morphology, which is crystalline at room temperature.

3. Results

3.1. Influence of the comonomer content on thermal behaviour and morphology

The short branches in ethylene–1-alkene copolymers, which disrupt the main chain regularity, give rise to an *ethylene sequence length distribution*. During crystallisation, sequences of equal length are sorted [38–40], leading to a *crystallisation temperature distribution* and a *distribution in the crystallite dimensions*, as reflected in the crystallisation range in DSC cooling curves. These crystallites with different dimensions will melt at different temperatures during heating, resulting in a *melting temperature distribution*, as reflected in the (broad) DSC heating curves. Clearly, short chain branches in homogeneous ethylene copolymers have a predominant effect on crystallisation and melting, as is reflected not only in the crystallisation/melting temperatures, but also in the (temperature-dependent) degree of crystallinity, the density at room temperature, the (temperature-dependent) properties of the material, etc.

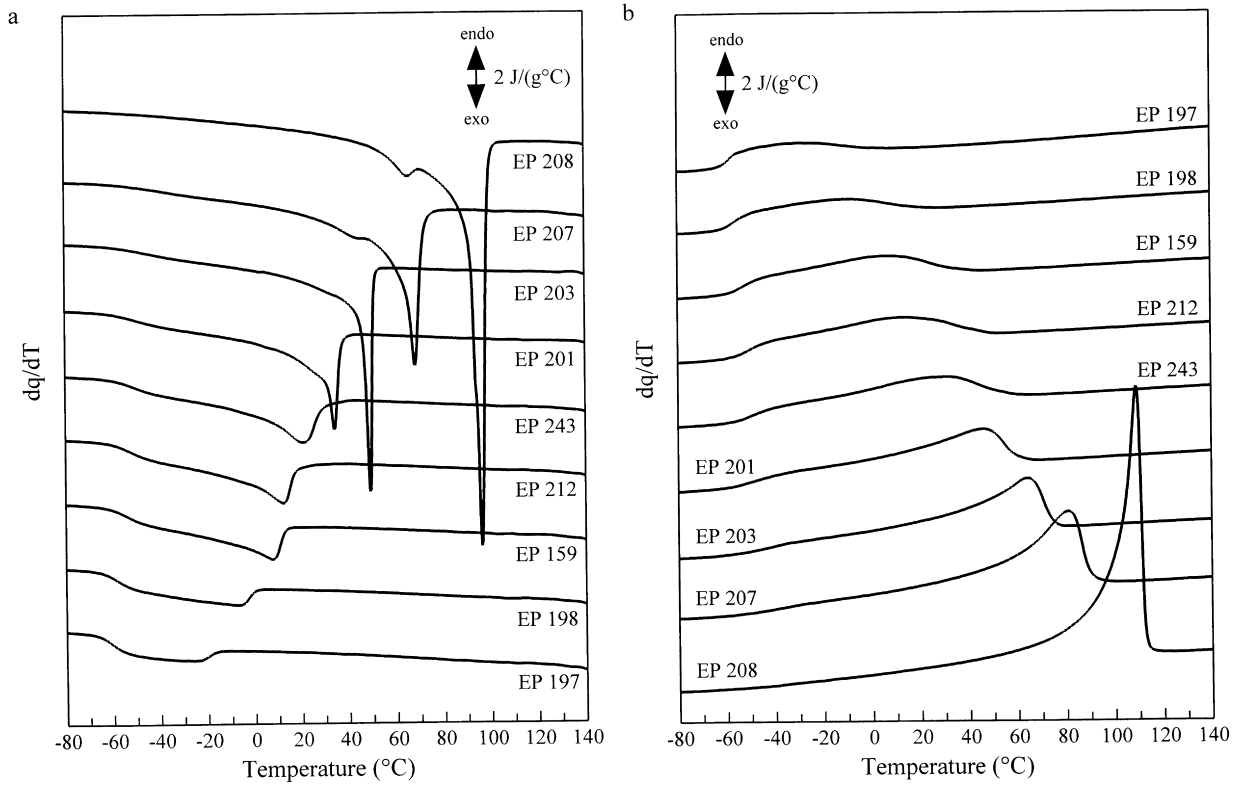

Fig. 1. (a) Cooling and (b) heating curves of homogeneous ethylene–propylene copolymers; rate 10°C/min. The curves have been displaced along the ordinate for better visualisation.

The crystallisation and melting behaviour of the homogeneous ethylene–propylene (EP) and ethylene–1-butene (EB) copolymers investigated by DSC are shown in Figs. 1 and 2, respectively. In case of the copolymers with the lowest comonomer contents a small peak in the cooling curves can be observed at about 30°C below the main exotherm. This small exotherm has tentatively been ascribed to homogeneous nucleation [1]. In Fig. 3 the crystallisation and melting peak temperatures (T_c^{peak} and T_m^{peak}), the glass transition temperatures (T_g) and the crystallinities at 23°C (w^c(23°C)) are plotted as a function of comonomer content. The influence of increasing comonomer content on thermal behaviour is observed in different ways.

Firstly, the DSC curves in cooling and heating become

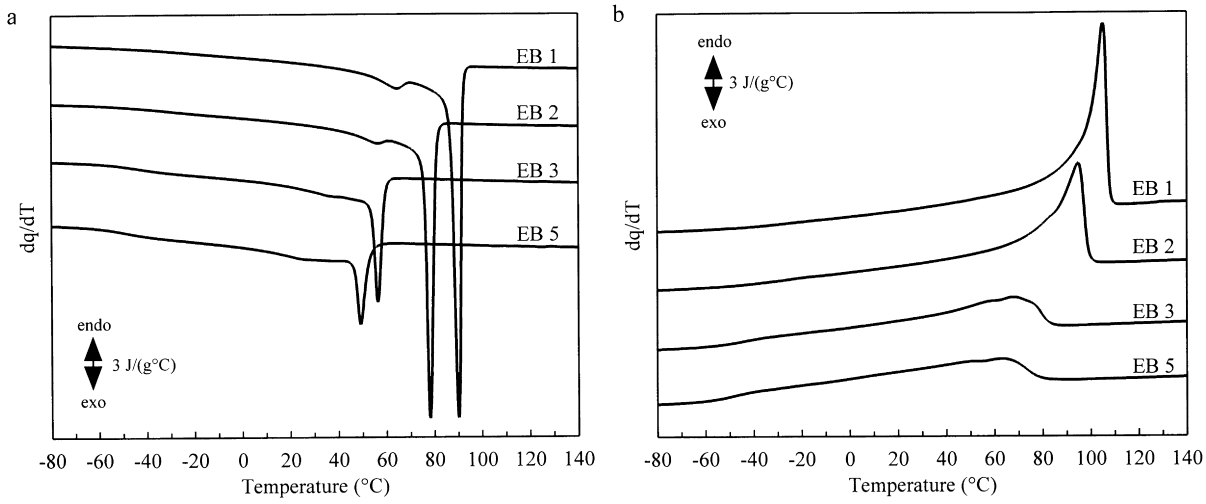

Fig. 2. (a) Cooling and (b) heating curves of homogeneous ethylene–1-butene copolymers; rate 10°C/min. The curves have been displaced along the ordinate for better visualisation.

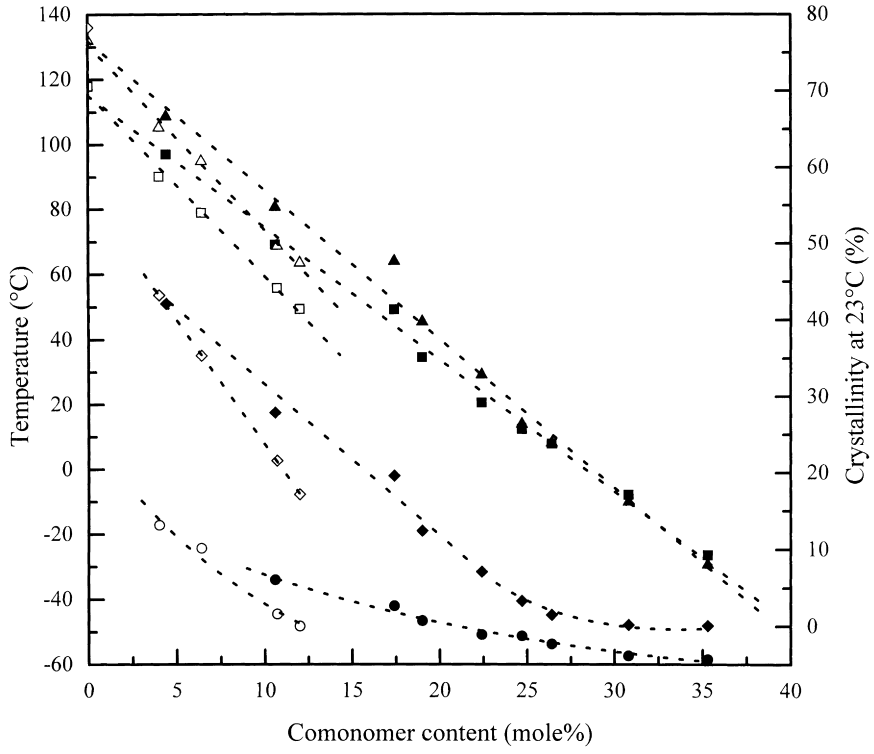

Fig. 3. Thermal characteristics of JW 1114 and EP (solid symbols) and EB (open symbols) copolymers obtained from DSC measurements in heating at 10°C/min after cooling at the same rate: left ordinate: T_c^{peak} (squares), T_m^{peak} (triangles), T_g (circles); right ordinate: w^c at 23°C (diamonds).

broader and flatter and shift to lower temperatures. For the highest comonomer contents crystallisation and melting approach the glass transition region. T_c^{peak} and T_m^{peak} reveal a nearly linear relationship to the comonomer content (Fig. 3), as is also observed below for T_x^{eo} and T_x^{ro}. At high propylene contents (>30 mole) a switch in the relative position of T_c^{peak} and the corresponding T_m^{peak} is observed. This feature can be ascribed to the very broad and flat DSC signal at high comonomer contents, which leads to a less accurate or even hardly possible peak determination.

Secondly, the DSC peak areas become smaller indicating lower crystallinities.

Thirdly, (de)vitrification takes place at decreasing temperatures, leading to decreasing T_g values while the stepwise change in dq/dT, reflecting (de)vitrification, is more pronounced at high comonomer contents. The decrease of T_g

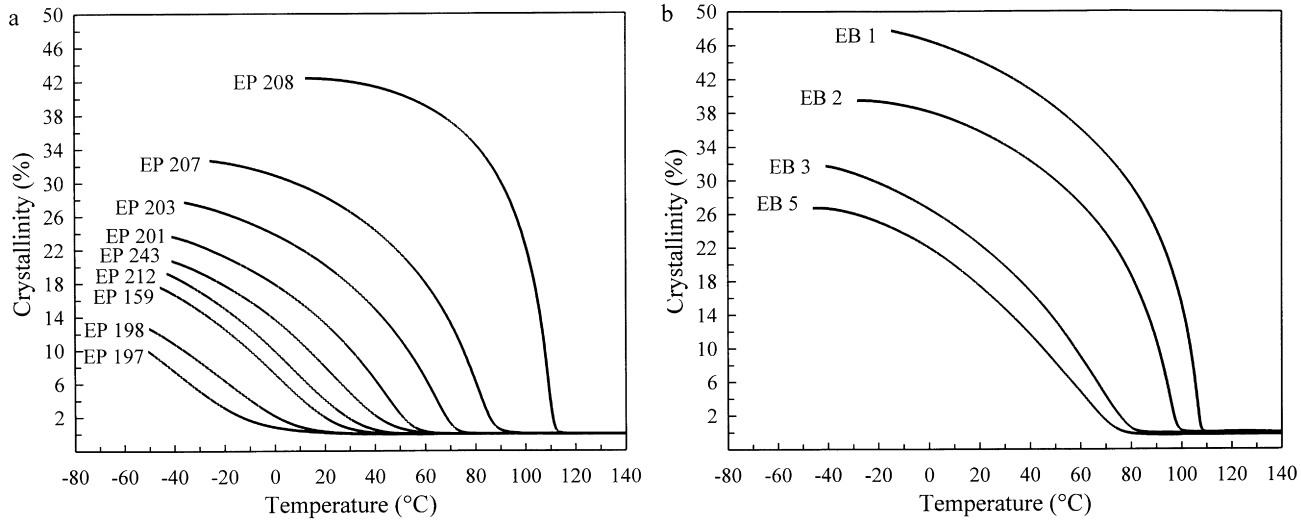

Fig. 4. Crystallinity of homogeneous (a) EP and (b) EB copolymers as a function of temperature, calculated from DSC heating curves after cooling (all at 10°C/min) by extrapolation from the melt.

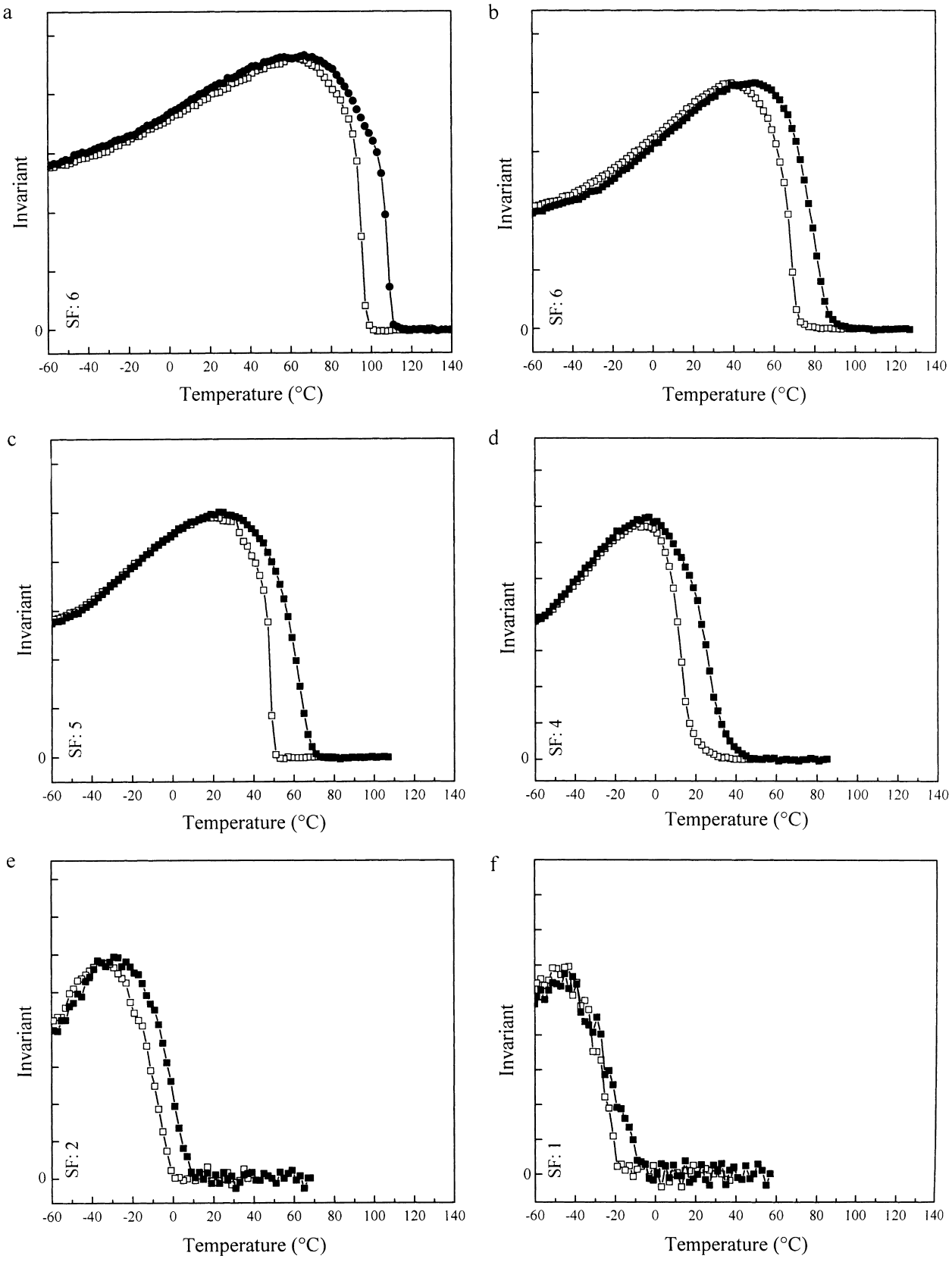

Fig. 5. SAXS invariants of homogeneous EP copolymers in cooling (□) and subsequent heating (■) at 10°C/min: (a) EP 208; (b) EP 207; (c) EP 203; (d) EP 212; (e) EP 198; (f) EP 197; arbitrary invariant scale, but comparable using the scale factors (SF) given.

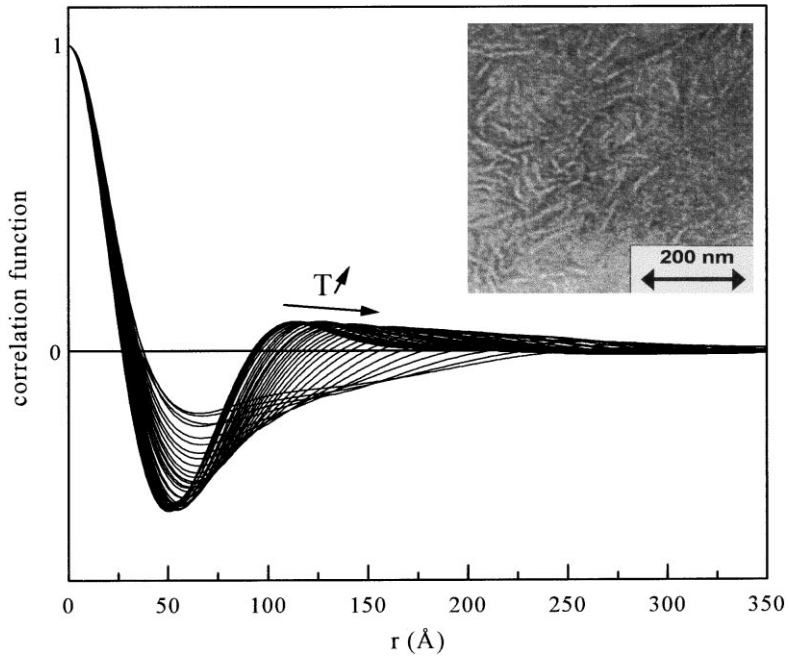

Fig. 6. Linear correlation functions of EB 2 (cooled at −1°C/min) during heating from 25 to 91°C at 10°C/min, with corresponding TEM picture [3] at room temperature.

levels off at a certain comonomer content, as shown in Fig. 3. This can be interpreted as one side of a minimum [41]. With a further increase in comonomer content, the T_g would evolve to that of the homopolymer of the comonomer, which is approximately −10°C for polypropylene and −25°C for poly-1-butene.

The observation of broadening DSC curves, lowering transition temperatures and decreasing DSC peak areas with increasing comonomer content can be explained by the fact that a larger amount of branches, caused by the higher comonomer content, reduces the capability to crystallise by shortening the length of the crystallisable ethylene sequences. As a result, crystallisation takes place at progressively lower temperatures, where chain mobility decreases as well. Hence, the chain segments are hindered to find sequences of same length and smaller, less perfect and less stable crystallites will form during crystallisation [3,10,38–40]. Both effects result in lower crystallinities with increasing comonomer content, as confirmed by the decreasing peak areas. Crystallinities as a function of temperature during heating, calculated from the DSC heating curves of the EP and EB copolymers (Figs. 1b and 2b), are shown in Fig. 4a and b, respectively. Good agreement is found with the results obtained from heat capacity measurements by Mathot et al. [3]. During cooling from the melt, as soon as crystallisation starts, the crystallinity increases until it reaches a maximum value just above the glass transition. In subsequent heating such a maximum value is the "initial crystallinity" value which decreases during melting.

The thermal behaviour of the EP copolymers revealed by the invariants as calculated from the time-resolved SAXS measurements is shown in Fig. 5. When the copolymer is in the melt the invariant vanishes, as a result of the absence of macroscopic electron density fluctuations (see Eq. (4)). The maxima in the SAXS invariant result from the combined temperature dependencies of the terms $\phi_L(1-\phi_L)$ and $(d_c-d_a)^2$, because all crystallinities are below 50%. With increasing comonomer content the on- and offset of the invariant during cooling and heating shift to lower temperatures and the scattered intensity drops because of the reduced crystallinity and density differences. The invariants during cooling and heating do not overlap due to hysteresis effects. For crystallisation nuclei have to be formed, leading to an undercooling, while this is not the case for melting. The SAXS-invariant of all copolymers, even the one with the lowest density, changes during cooling and heating. This means that in all case electron density fluctuations are still present in the sample and that the electron densities of the *crystallised units* are still sufficiently higher than those of their surroundings to be detected. This finding, in addition to the good agreement with the crystallisation onset and melting offset temperatures observed in DSC (see Fig. 4), illustrates the consistency between SAXS and DSC [3]. All copolymers reveal a maximum in the SAXS curve, which indicates the presence of electron density fluctuations that gives rise to a correlation maximum. With increasing comonomer content the intensity of this maximum decreases and its position moves to higher *s*-values.

For the copolymers with the lowest comonomer contents, revealing a lamellar morphology in TEM (i.e. fulfilling of the basic assumption mentioned before), a linear correlation function analysis was performed to obtain information about some morphological parameters. The linear correlation functions of EB 2 (previously cooled at −1°C/min to

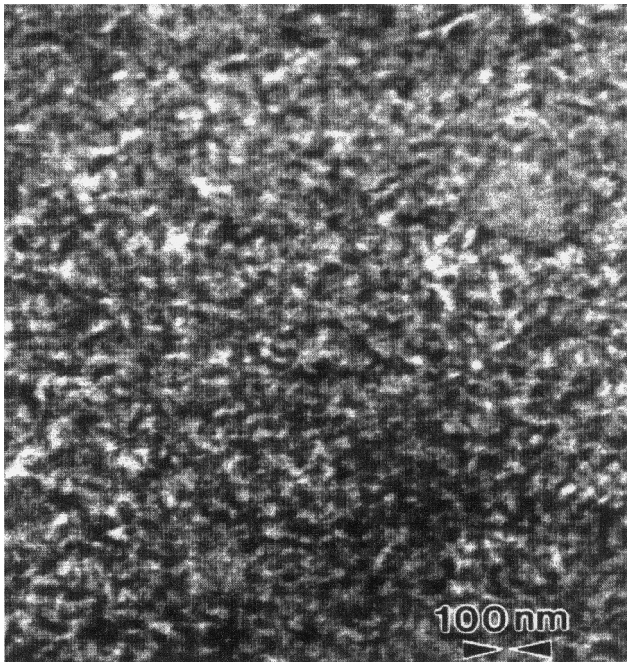

Fig. 7. TEM micrograph [3] of EP 203: granular base morphology.

room temperature) during heating at 10°C/min are shown in Fig. 6 together with the corresponding TEM picture, revealing the lamellar morphology. In case of the very-low-density (≤ 870 kg/m^3 at room temperature) copolymers, which reveal a granular morphology in TEM (Fig. 7), the linear correlation function approach is not applicable any longer and only the SAXS-invariant during cooling and heating can be used. The temperature-dependence of the long period (LP), the crystalline lamellar thickness (L_c), the amorphous layer thickness (L_a) and the volume crystallinity (ϕ_L) of EB 2 during heating at 10°C/min are illustrated in Fig. 8. LP and L_a increase with temperature, while L_c remains constant around 45 Å. The sharper increase of the long period at high temperatures indicates that besides surface melting some full strand melting also occurs [8]: groups of crystalline lamellae melt as a whole giving rise to larger amorphous regions.

The static WAXD patterns of the EP and EB copolymers, cooled at −10°C/min to room temperature and quenched from the melt to −70°C with subsequent heating to room temperature, are shown in Figs. 9 and 10. The three fitted Pearson peaks of the quenched EP 208 are also inserted in Fig. 9b. The experimental curve and the overall peak fitting are identical.

The diffraction pattern of the branched copolymers, like that of linear PE, consists of the crystalline orthorhombic 110- and 200-reflections superimposed on a broad amorphous halo. With increasing comonomer content the crystalline reflections become less pronounced and finally become undetectable, while the amorphous halo intensifies (intensities are in arbitrary units, a.u., but comparable) and becomes sharper. In case of the quenched samples, the crystalline reflections are less pronounced compared to those of the more slowly cooled sample. Obviously, quenching leads to smaller and less perfect crystallites and a lower crystallinity. For copolymers with densities below approximately 870 kg/m^3 at room temperature no clear crystalline reflections can any longer be observed at room temperature. This is for example the case for EP 243, which is semi-crystalline according to DSC ($w^c_{23°C}$(DSC) ≠ 0; see Figs. 1 and 4, both in cooling and heating), while in WAXD only an amorphous halo is observed ($w^c_{23°C}$(WAXD) = 0; see Fig. 9, both

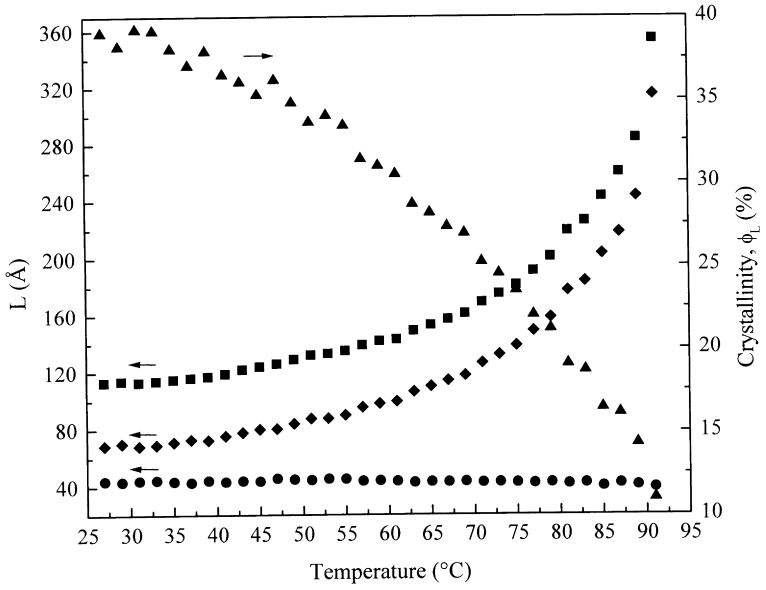

Fig. 8. Morphological parameters obtained from the linear correlation function analysis of the SAXS-data of EB 2 (cooled at −1°C/min to room temperature) during heating at 10°C/min: LP (■), L_a (◆), L_c (●) and ϕ_L (▲).

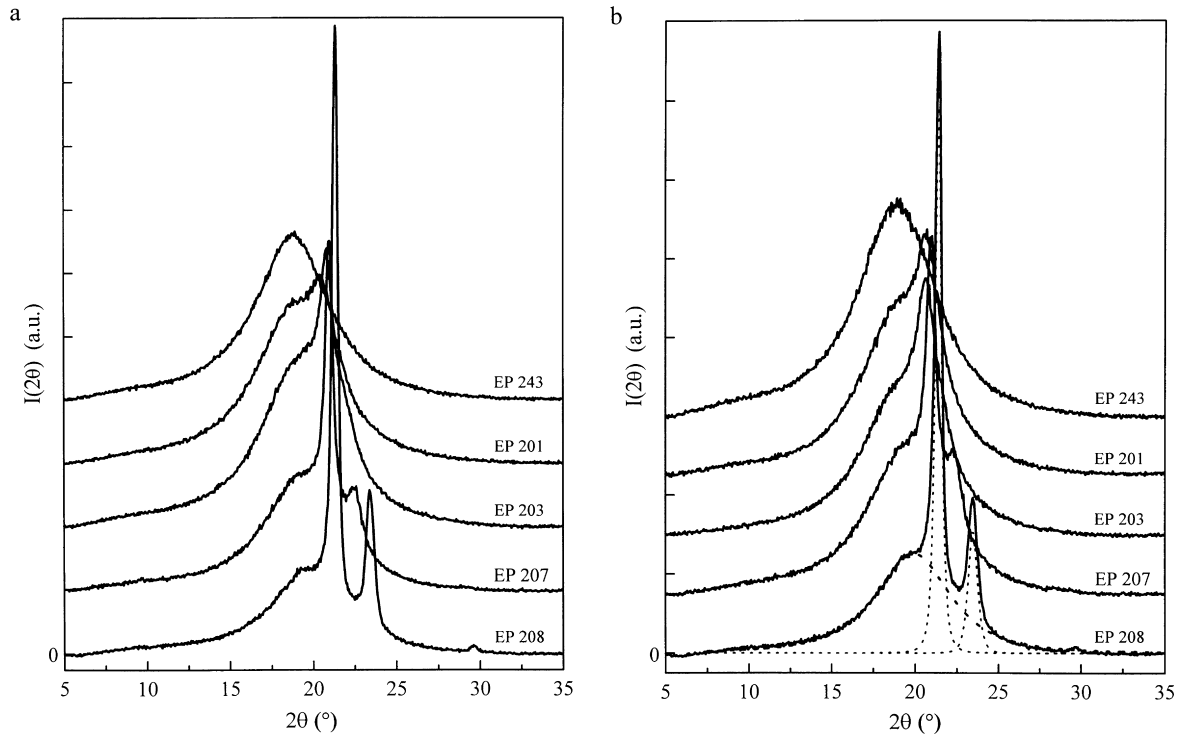

Fig. 9. WAXD patterns at room temperature of homogeneous EP copolymers (a) cooled from the melt at −10°C/min and (b) quenched from the melt to −70°C followed by heating; (···) fitted peaks. Successive patterns of the slowly cooled and quenched samples have been displaced by 2000 or 1500 units, respectively, along the ordinate for better visualisation.

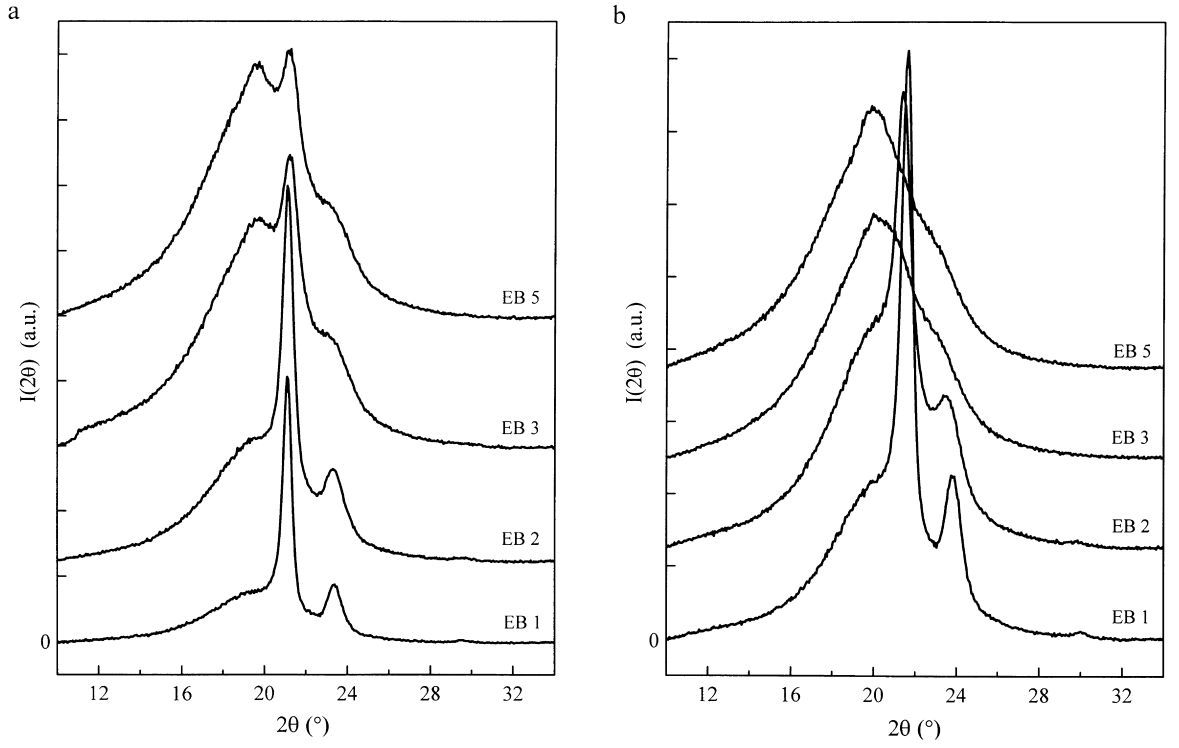

Fig. 10. WAXD patterns at room temperature of homogeneous EB copolymers (a) cooled at −10°C/min from the melt and (b) quenched from the melt to −70°C followed by heating. Successive patterns of the slowly cooled samples have been displaced by 5000, 7000 and 8000 units along the ordinate for better visualisation; for the quenched samples the displacement is 5000 units.

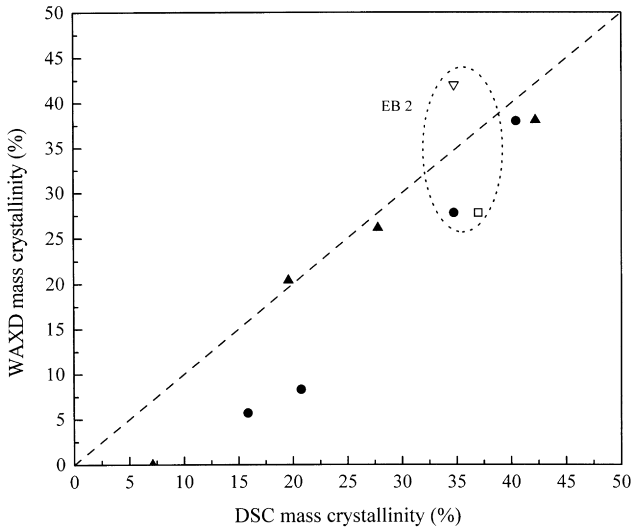

Fig. 11. Comparison of WAXD and DSC mass-crystallinities at room temperature of the homogeneous EP (▲) and EB (●) copolymers after cooling at 10°C/min from the melt; (▽) w^c of EB 2 from SAXS and (□) w^c of EB 2 from WAXD and c_p [3].

after cooling at 10°C/min and after quenching followed by heating). Obviously, this difference is caused by the fact that small and/or imperfect crystallites are formed during crystallisation which are no longer detectable by WAXD.

In Fig. 11 the mass crystallinities at room temperature of the EP and EB copolymers (cooled at −10°C/min from the melt) estimated from WAXD (Eq. (7)) are compared with those calculated from DSC results using Eq. (1). The mass crystallinities of EB 2 obtained from SAXS (Eqs. (5) and (6)) and c_p measurements [3] are also inserted in Fig. 11 for comparison. The figure illustrates that for the EP copolymers the DSC and WAXD crystallinities correspond at crystallinities above 20%, while for the EB copolymers the agreement only exists at the highest crystallinity (~40%). At lower crystallinities (increasing comonomer content) the data diverge. This is probably due to the decreasing sensitivity of WAXD because of the tendency towards smaller and/or imperfect crystallites leading to crystalline reflections which may no longer be detectable. Further, the mass crystallinity of EB 2 obtained from SAXS is about 7% higher compared to DSC, while the one obtained from WAXD is about 7% lower. The difference between the crystallinity obtained from c_p measurements (37%) [3] and from DSC using the extrapolation method (35%) is within the experimental error. The high SAXS-crystallinity can be ascribed to the fact that *local* crystallinities *in the semi-crystalline regions* are involved, while DSC is related to the *bulk* crystallinity. The low WAXD-crystallinity is due to the limited sensitivity, as mentioned above.

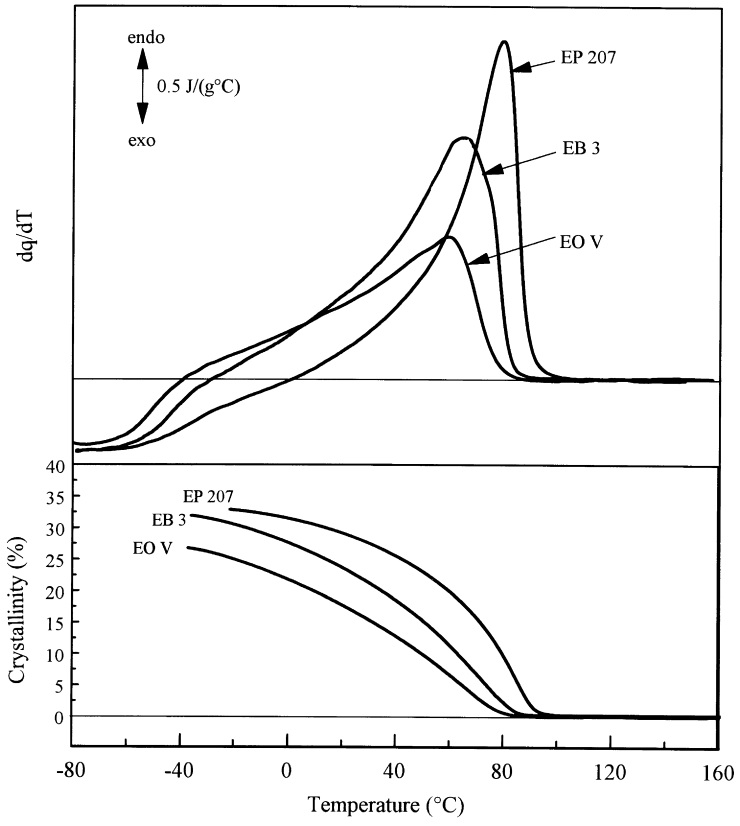

Fig. 12. DSC heating curves and corresponding crystallinities after cooling (all at 10°C/min) of homogeneous EP, EB and EO copolymers of nearly the same comonomer content (approximately 11 mole %).

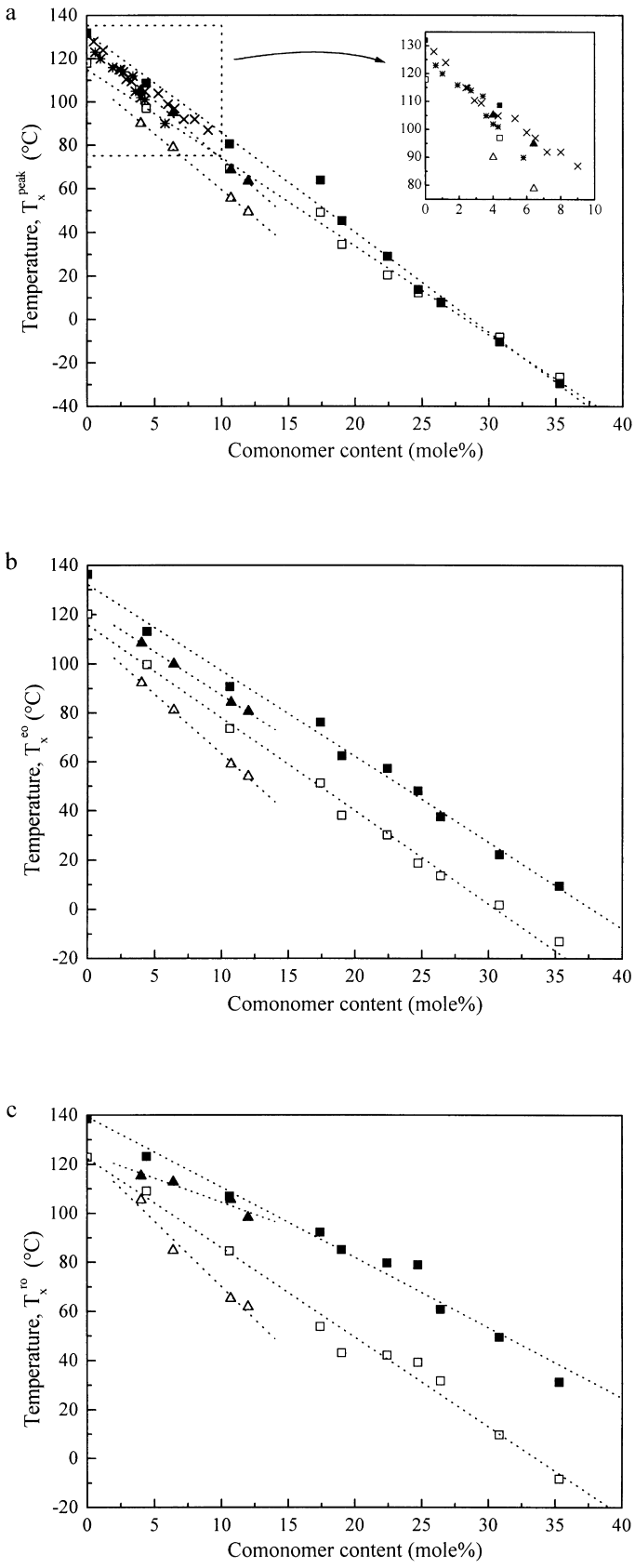

Fig. 13. Crystallisation (open symbols) and melting (solid symbols) temperatures of JW 1114 and homogeneous EP (squares) and EB (triangles) copolymers defined by three different ways: (a) T_x^{peak}; (b) T_x^{eo}, (c) T_x^{ro}; (×) T_m^{peak} EB after Clas et al. [20], (*)T_m^{peak} EB after Alamo et al. [42].

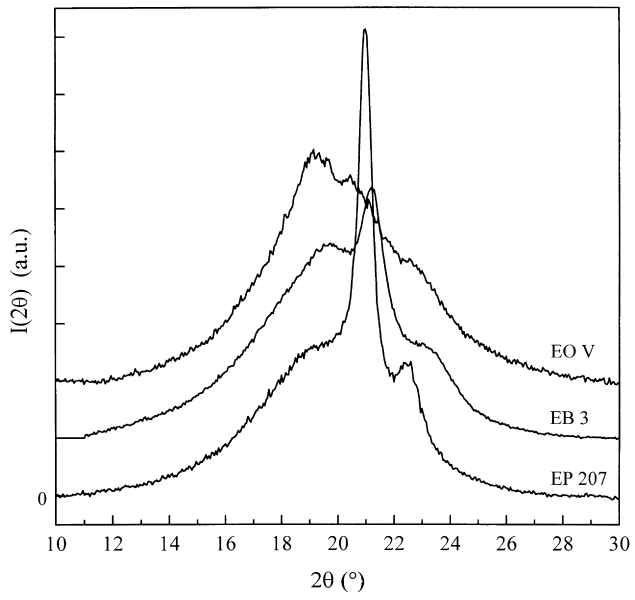

Fig. 14. WAXD patterns at room temperature of EP 207, EB 3 and EO V (appr. 11 mole%). Successive patterns have been displaced by 2000 units along the ordinate for better visualisation.

3.2. Influence of comonomer type on thermal behaviour and morphology

The length of the short-chain branching, which is controlled by the comonomer used during the synthetic step, determines whether or not it will be incorporated in the crystalline regions and, hence, will have an influence on morphology and thermal properties. It is generally accepted that the methyl branches can be incorporated in an interstitial position [12–14], which gives rise to distorted lamellae, whereas hexyl branches are absolutely rejected from the crystalline core. Ethyl branches have an intermediate behaviour influenced by the cooling rate.

Fig. 12 shows the DSC heating curves and the corresponding crystallinities of EP 207, EB 3 and EO V [3]. These three copolymers, which all have a comonomer content around 11 mole% are synthesised using different types of comonomer (propylene, 1-butene and 1-octene, respectively). The influence of increasing branch length on the thermal behaviour is similar to the influence of increasing comonomer content: broader and flatter DSC curves and shift of T_m, T_c and T_g to lower temperatures. At temperatures above 0°C the peak area becomes smaller at higher branch length, indicating a decreasing crystallinity. At lower temperatures just above the T_g, however, the influence of the branch length on the crystallinity is no longer obvious. This can be illustrated using the extrapolation method in which the area above the line reflecting extrapolation from the melt is added, while the area below the line is subtracted (see text after Eq. (1)). It seems that at temperatures just above T_g the maximal crystallinities of the EP and EB copolymers reach the same values, while the difference with the EO copolymer is nearly constant. It could, of course, also be argued that the relatively low maximum for the crystallinity of the EP copolymer is caused by the hindering of crystallisation by vitrification at relatively high temperatures.

The crystallisation and melting temperatures of JW 1114 and the EP and EB copolymers, defined as the peak temperatures of the DSC exo- and endotherms (T_x^{peak}), as the extrapolated on/offset (T_x^{eo}) and as the real on/offset (T_x^{ro}), are plotted as a function of the comonomer content

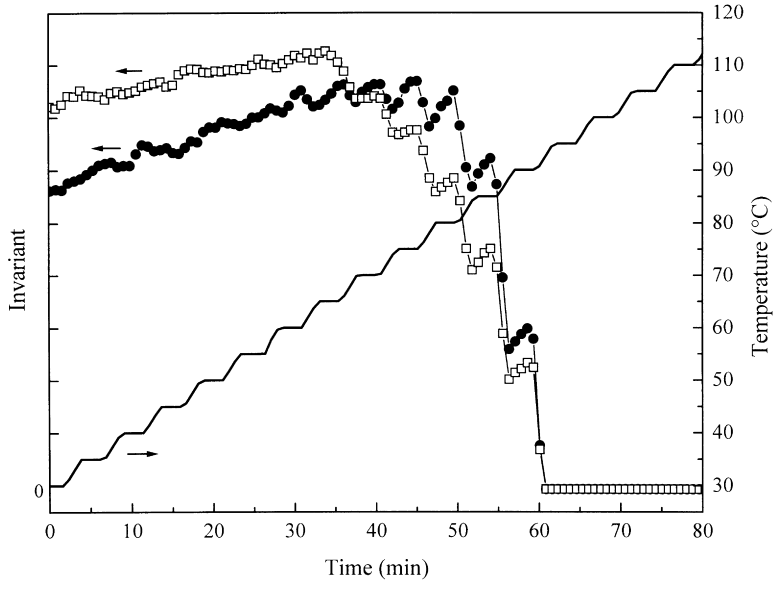

Fig. 15. SAXS-invariant of EB 2, previously cooled at −1°C/min (□) or quenched from the melt (●), during a scan-iso temperature–time heating program (arbitrary invariant scale, but comparable); (—) temperature.

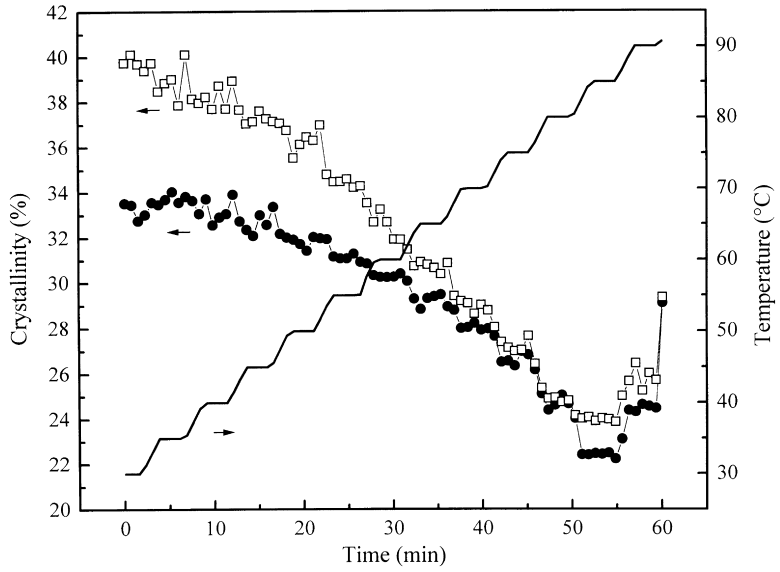

Fig. 16. ϕ_L of EB 2 cooled at −1°C/min (□) or quenched (●) from the melt during a scan-iso temperature–time program; (—) temperature.

in Fig. 13a, b and c, respectively. The data (T_m^{peak}) obtained by Clas et al.[20] (× symbols) and Alamo et al. [42]. (* symbols) are inserted in Fig. 13a for comparison. Fig. 13 shows that, irrespective of the determination method and within the range of comonomer contents studied, the crystallisation and melting temperature decrease approximately linearly with increasing comonomer content. This effect becomes more pronounced (sharper decrease) at higher branch length. These observations agree with the ability of the methyl branches to be incorporated in the crystal structure [12–14]. In case of T_x^{peak} the difference between T_m and T_c ($\Delta T = T_m - T_c$) is relatively small and becomes zero at the highest comonomer contents. In contrast, the ΔT of T_x^{eo} is larger and increases with the comonomer content; this effect is even more pronounced in case of T_x^{ro}.

Agreement is found with the T_m^{peak}-values of EB copolymers obtained by Clas et al. using a comparable catalyst system and a heating rate of 20°C/min. The results of Alamo et al. are somewhat lower, probably because the melting peak temperatures of rapidly crystallised random EB copolymers are involved.

TEM pictures [3] of copolymers having the same comonomer content reveal a morphology change with increasing

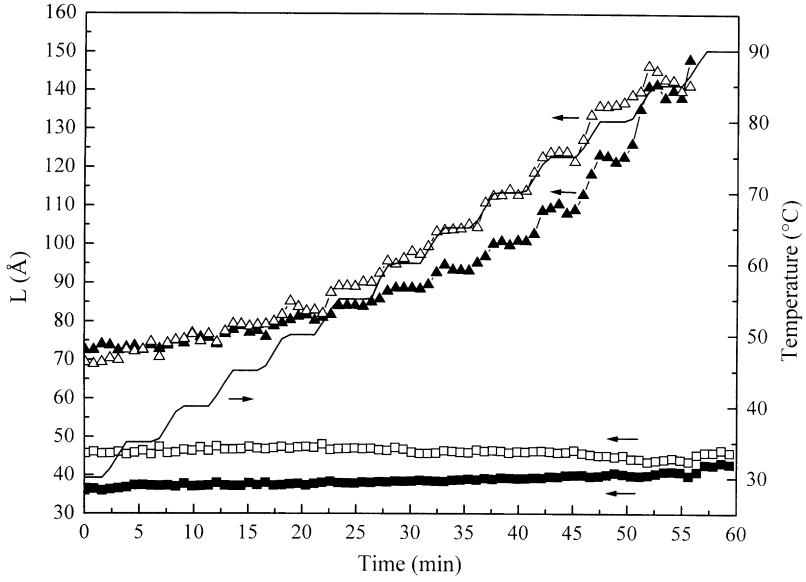

Fig. 17. L_a (triangles) and L_c (squares) of EB 2 cooled at −1°C/min (open symbols) and EB 2 quenched from the melt (solid symbols) during the scan-iso heating run; (—) temperature.

branch length from a lamellar base morphology with some granular structures present too (EP 207) into a granular base morphology with very few isolated lamellae (EO V).

The difference in morphology is also reflected in the WAXD patterns at room temperature of EP 207, EB 3 and EO V, as presented in Fig. 14. With increasing branch length at a certain comonomer content, the crystalline orthorhombic 110- and 200-reflections become less pronounced and the ratio of the scattered area of the crystalline peaks to the total area (i.e. crystallinity) decreases.

3.3. Metastability (scan-iso)

Fig. 15 shows the SAXS invariant, Q_{id}, of EB 2 previously cooled at -1°C/min or quenched from the melt, during a scan-iso-temperature–time program. The SAXS-invariant is strongly influenced by the stepwise temperature–time program: Q_{id} increases during the isothermal periods, as can be clearly observed above 75°C. After correction for the temperature dependencies of d_c, d_a and ϕ_L, it appears that the increase during the isothermal periods is probably caused by an increasing fraction of semi-crystalline regions [43] (α_s, see Eq. (4)), resulting for instance from lateral growth and/or the formation of new semi-crystalline regions. ϕ_L of the quenched and the slowly cooled EB 2 sample are shown in Fig. 16 as a function of temperature. ϕ_L decreases during the heating scans, as a result of melting, and remains constant during the isothermal periods, while an overall decrease is observed till 80°C. The behaviour during the isothermal periods can be interpreted as the combination of melting and recrystallisation. Only at the highest temperatures an increase in the local crystallinity is seen, which can be ascribed to the appearance of an amorphous fraction in the final melting region. Only the remaining semi-crystalline regions with a relatively high internal crystallinity persist up to the highest temperature and contribute to the observed scattering [8]. At low temperatures, ϕ_L of the slowly cooled sample is obviously higher than that of quenched EB 2. However, as the temperature is raised, ϕ_L of the quenched sample approaches that of the slowly cooled sample and the values become identical around 70°C. This "overtaking" effect can be ascribed to fast reorganisation in the quenched sample during heating. The tendency of the quenched sample to reorganise during heating is understandable because during quenching only relatively small and imperfect crystallites are formed involving the cocrystallisation of ethylene sequences of different lengths. According to Goderis et al. [44], such crystals repeatedly melt and recrystallise during heating over almost the entire melting range.

The scan-iso heating program also influences L_a, as shown in Fig. 17. L_a follows the scan-iso temperature profile rather closely: it increases during the heating scans and remains nearly constant during the isothermal periods. In contrast, there is hardly any influence of the scan-iso heating program on L_c, as illustrated in Fig. 17. The quenched sample reveals a very slight overall increase, while L_c of the slowly cooled sample remains more or less constant around 46 Å. Good agreement is found in the L_a- and L_c-values of slowly cooled EB 2 at the start of the scan-iso heating (Fig. 17) and the linear heating (Fig. 8) measurements, which also illustrates the reliability of the measurements and the analysis. The difference between the lamellar thickness observed in the SAXS measurements (about 46 Å) and the thickness according to the TEM micrographs [3] (about 75 Å) suggests that TEM reveals the high side of the lamellar thickness distribution.

These results imply that in EB 2 considerable structural changes occur within a few minutes during the isothermal periods. Therefore, static WAXD and SAXS measurements are less meaningful in this temperature range. Even in dynamic measurements a considerable degree of reorganisation is expected.

4. Discussion

The results confirm the well-known fact that the comonomer content has a major influence on the crystallisation and melting behaviour and morphology of copolymers [1,42]. The length of the side branch, as determined by the comonomer type used in the synthetic step, also has an influence because the branches may or may not be incorporated in the crystallites, as remarked before.

It is clear that compared to heterogeneous copolymers, such as LLDPEs and VLDPEs, homogeneous copolymers like the ones discussed here, are much simpler in terms of structure, crystallisation and melting behaviour and morphology. The use of a catalyst with a single active site during the synthetic step results in a statistical distribution in all chains and leads to intra- and intermolecularly homogeneous copolymers. The statistics of the EP copolymers studied turned out to be in-between alternating and random, with a product of copolymer reactivity ratios, $r_e r_p$, of about 0.50 [45]. These copolymers are characterised by single-peaked ethylene sequence length distributions [3,45–47] (ESLDs) and single-peaked DSC curves [1].

When the comonomer content increases, gradual changes are observed in the thermal behaviour and the morphology. The experimental results do not reveal any discontinuities. With increasing branching content, it can be expected that crystallisation into lamellar structures via the conventional chain folding mechanism [48] would be increasingly hindered. The lateral dimensions of the lamellae decrease gradually until they reach the order of magnitude of the longitudinal dimension. Hence, the morphology changes gradually from a lamellar base morphology into a granular base morphology (small, blocky structures) at high comonomer contents. At certain comonomer contents both morphologies can occur simultaneously [3,49]. This is caused by the fact that the ethylene copolymers under investigation have broad ESLDs—due to the chain growth

statistics—and, hence, contain ethylene sequences of very different lengths. Apparently the comonomer contents of some copolymers are such that the longest ethylene sequences are sufficiently long to fold into lamellae, while the shortest sequences can only form granular or blocky structures. The reduction in the lateral dimensions of the crystallites at higher comonomer contents can be ascribed to two effects. When the number of side branches in increased, the crystallisation process shifts to lower temperatures reaching the glass transition region in case of the highest comonomer contents. Consequently the mobility of the chain segments is reduced, resulting in a more difficult diffusion of the ethylene sequences towards the crystal growth fronts. The higher degree of supercooling, however, increases the driving force for crystallisation and decreases the critical dimensions for a stable nucleus, enabling the shorter ethylene sequences to crystallise too. Undoubtedly, this will lead by cocrystallisation to the linkage in the crystallites of sequences of unequal length at higher comonomer contents. Because of the concomitant crowding of emerging non-crystallised chain segments, the lateral growth of the crystallites will be frustrated, leading to the granular structures mentioned above, or, at still higher comonomer contents even to a fringed-micelle type of morphology. In case of the copolymers with the highest comonomer contents, where crystallisation occurs just above the glass transition region, one can imagine that only the nearest-neighbour segments can crystallise [50]. This possibly results in a morphology characterised by *clusters of loosely packed ethylene sequences*, as suggested by Monte-Carlo simulations [3,51].

The gradual decrease and disappearance of the crystalline reflections in WAXD at higher comonomer contents can be explained by the decrease in constructive interference due to progressively smaller and less perfect crystallites formed during crystallisation. At a density of approximately 870 kg/m^3 and below, no crystalline reflections can be detected any longer at room temperature. Further, one should notice the sharpness of the amorphous halo in case of copolymers with high comonomer contents. Some authors [52–54] assume that this sharpness is due to the superposition of two diffraction peaks of two different phases: a liquid-like phase (as in the melt) and a more-ordered fraction which is better packed than a liquid, but more loosely packed than a usual orthorhombic crystallite.

All copolymers reveal a change in the SAXS-invariant during cooling and heating, even the ones with very low crystallinities (high comonomer contents). This means that in all cases—including that of a cluster type of morphology—the electron densities of crystalline structures are definitely higher than their surroundings.

As already mentioned, an ESLD can lead to different morphologies [3,49] in one and the same sample. One should, however, be aware of the fact that not all these morphologies have been experimentally demonstrated. Techniques are available to observe lamellar and granular structures. Fringed-micelle structures and clusters, on the other hand, are still assumptions and suggestions, so there is every reason to be cautious.

5. Conclusions

Increasing comonomer content and branch length have important—and to some extent similar—influences on the thermal behaviour of homogeneous ethylene–propylene and ethylene–1-butene copolymers. The DSC melting and crystallisation curves become broader and flatter, the melting and crystallisation temperatures shift to lower temperatures, the glass transition becomes more pronounced and the glass transition temperature decreases and the peak area becomes smaller indicating a lowering crystallinity. With increasing comonomer content, the observations reflect dimension distributions of increasingly small and/or less perfect crystalline structures of low thermal stability.

The orthorhombic crystalline 110- and 200-reflections in WAXD become less pronounced as the comonomer content is increased and are no longer detectable at room temperature when the density at room temperature of the copolymer reaches values below approximately 870 kg/m^3. This can be ascribed to the presence of crystalline structures, which are too small and/or too imperfect to produce detectable constructive interference in WAXD.

All copolymers reveal a change in the SAXS-invariant during cooling and heating, with hysteresis effects typical for crystallisation and melting of polymers. This means that, even in the copolymers with the highest comonomer contents or lowest densities, crystalline entities are present with electron densities that differ sufficiently from the amorphous surroundings. Good agreement is found between the crystallisation onset and melting offset temperatures obtained by DSC and SAXS.

A linear correlation function analysis of the SAXS-data of the EB copolymer revealing a lamellar morphology in TEM, shows an increase of the long period and the amorphous layer thickness with temperature, while the crystalline lamellar thickness remains constant.

The scan-iso SAXS experiment shows that in an ethylene–1-butene copolymer with 6.4 mole% 1-butene a considerable degree of instantaneous reorganisation occurs during dynamic (heating) and static (isothermal) measurements. The observed reorganisation phenomena are probably due to a combination of melting and recrystallisation, rather than chain diffusion since the latter is hindered by the short-chain branches in the copolymer. These observations stress the importance of time-resolved measurements.

It should be emphasised that the results of the different techniques presented here reveal no discontinuities with increasing comonomer content. By TEM, with increasing comonomer content, a gradual change is seen from a lamellar base morphology into a granular one consisting of small, imperfect blocky structures. When increasing the

comonomer content, the changes in the resulting morphology can be summarised as follows: lamellar stacks organised in spherulitic superstructures → isolated lamellae (no spherulites) and decrease of the lateral dimensions of the lamellae → granular morphology (small blocky structures) → clusters or loosely packed ethylene sequences (?) as suggested by Monte-Carlo simulations [3,51]. It should be kept in mind that these morphology changes occur gradually and that, even in homogeneous copolymers, different morphologies can be present simultaneously.

Acknowledgements

This research was financially supported by the Research Council K.U.Leuven, the Fund for Scientific Research Flanders (F.W.O.-Vlaanderen) and DSM Research (Geleen). One of the authors (S.V.E.) is indebted to the Flemish Institute for the Promotion of Scientific and Technological Research in Industry (I.W.T.) for a fellowship. V. Mathot—on leave from DSM Research, Geleen, The Netherlands—is indebted to the K.U. Leuven for a guest professorship. We thank the European Union for support of the work at EMBL Hamburg under the TMR/LSF program (ERBFMGECT980134).

References

[1] Mathot VBF, editor. Calorimetry and thermal analysis of polymers. New York: Hanser Publishers, 1994. chap. 9, p. 231.
[2] Mathot VBF, Scherrenberg RL, Pijpers MFJ, Bras W. J Thermal Anal 1996;46(3–4):681.
[3] Mathot VBF, Scherrenberg RL, Pijpers MFJ, Engelen YMT. In: Hosoda S, editor. The new trends in polyolefin science and technology. Publisher Research Signpost, 1996. p. 71.
[4] Mathot VBF, Scherrenberg RL, Pijpers MFJ. Polymer 1998;39(19):4541.
[5] Defoor F, Groeninckx G, Schouterden P, Van der Heijden B. Polymer 1992;33(18):5186.
[6] Peeters M, Goderis B, Vonk C, Reynaers H, Mathot V. J Polym Sci Polym Phys 1997;35:2689.
[7] Peeters M, Goderis B, Reynaers H, Mathot V. J Polym Sci Polym Phys 1999;37:83.
[8] Goderis B, Reynaers H, Koch MHJ, Mathot VBF. J Polym Sci Polym Phys 1999;37:1715.
[9] Reddy SS, Swaram S. Prog Polym Sci 1995;20(2):309.
[10] Bensason S, Minick J, Moet A, Chum S, Hiltner A, Baer E. J Polym Sci Polym Phys 1996;34:1301.
[11] Kravchenko R, Waymouth RM. Macromolecules 1998;31(1):1.
[12] Kortleve G, Tuijnman CA, Vonk CG. J Polym Sci Polym Chem 1972;10:123.
[13] Hosoda S, Nomura H, Gotoh Y, Kihara H. Polymer 1990;31:1999.
[14] Vonk CG, Reynaers H. Polymer Commun 1990;31:190.
[15] Wunderlich B. Vol. 3: Crystal melting. Macromolecular physics. New York: Academic Press, 1980. chap. 10, p. 235.
[16] Vanden Eynde S. Masters Thesis, Katholieke Universiteit Leuven, Belgium, 1995.
[17] Koberstein JT, Russell TP. J Polym Sci Polym Phys 1985;23:1109.
[18] Schouterden P, Groeninckx G, Reynaers H, Riekel C, Koch MHJ. Polym Bull 1985;13:533.
[19] Peeters M. PhD thesis, Katholieke Universiteit Leuven, Belgium, 1995.
[20] Clas S-D, McFaddin DC, Russell KE, Scammel-Bullock MV, Peat IR. J Polym Sci Polym Chem 1987;25:3105.
[21] Flynn JH. Thermochim Acta 1974;8:69.
[22] Moyhnihan CT, Esteal AJ, De Bolt MA, Tucker J. J Am Ceram Soc 1976;59:12.
[23] Richardson MJ, Savill NG. Br Polym J 1979;11:123.
[24] Mathot VBF, Pijpers MFJ. J Thermal Anal 1983;28:349.
[25] Mathot VBF, editor. Calorimetry and thermal analysis of polymers. New York: Hanser Publishers, 1994. chap. 5, p. 105.
[26] Mathot VBF. Polymer 1984;25:579 Errata: Mathot VBF. Polymer 1986;27:969.
[27] Wunderlich B, Czornyj G. Macromolecules 1977;10(5):906.
[28] Koch MHJ, Bordas J. Nucl Instrum Methods 1983;208:435.
[29] Gabriel A. Rev Sci Instrum 1977;48:1303.
[30] Mathot VBF, editor. Thermal analysis and calorimetry in polymer physics. Thermochim Acta 1994;238.
[31] Schick C, Höhne GWH, editors. Temperature modulated calorimetry. Thermochim Acta 1997;304/305.
[32] Scherrenberg R, Mathot V, Steeman P. Temperature modulated DSC. Judovits LH, Menczel JD, editors. J Thermal Anal 1998;54:477.
[33] Strobl GR, Schneider M. J Polym Sci Polym Phys 1980;18:1343.
[34] Koberstein J, Russell TP, Stein RS. J Polym Sci Polym Phys 1979;17:1719.
[35] Alexander LE. X-ray diffraction methods in polymer science. New York, Huntington: Krieger RE Publishing Company, 1979. p. 189.
[36] Swan PR. J Polym Sci 1960;42:525.
[37] Aggarwal SL, Tilley GP. J Polym Sci 1955;18:17.
[38] Flory PJ. J Chem Phys 1947;15(9):684.
[39] Flory PJ. Trans Faraday Soc 1955;51:848.
[40] Kilian HG. Thermal analysis and calorimetry in polymer physics. Mathot VBF, editor. Thermochim Acta 1994;238:113.
[41] Maurer JJ. Rubber Chem Technol 1965;38:979.
[42] Alamo RG, Mandelkern L. Thermal analysis and calorimetry in polymer physics. Mathot VBF, editor. Thermochim Acta 1994; 238:155.
[43] Vanden Eynde S, Goderis B, Mathot VBF, Koch MHJ, Reynaers H. Submitted for publication.
[44] Goderis B, Peeters M, Reynaers H, Koch MHJ, Bras W, Mathot VBF, Ryan AJ. Submitted for publication.
[45] Mathot VBF, Fabrie ChCM, Tiemersma-Thoone GPJM, Van der Velden GPM. J Polym Sci Polym Phys 1990;28:2509.
[46] Mathot VBF, Fabrie ChCM. J Polym Sci Polym Phys 1990;28:2487.
[47] Mathot VBF, Fabrie ChCM, Tiemersma-Thoone GPJM, Van der Velden GPM. Proceedings Int Rubber Conf (IRC), Kyoto, 15–18 October 1985. p. 334.
[48] Wunderlich B. Vol. 1: Crystal structure, morphology, defects. Macromolecular physics. New York: Academic Press, 1977.
[49] Minick J, Moet A, Hiltner A, Baer E, Chum SP. J Appl Polym Sci 1995;58:1371.
[50] Wunderlich B. Vol. 2: Crystal nucleation, growth, annealing. Macromolecular physics. New York: Academic Press, 1976. chap. 6, p.181.
[51] van Ruiten J, van Dieren F, Mathot VBF. In: Dosière M, editor. Crystallization of polymers. Dordrecht: Kluwer Academic, 1993. p. 481.
[52] Clas SD, Heyding RD, McFaddin DC, Russell KE, Scammel-Bullock MV. J Polym Sci Polym Phys 1988;26:1271.
[53] McFaddin DC, Russell KE, Wu G, Heyding RD. J Polym Sci Polym Phys 1993;31:175.
[54] Androsch R. Polymer 1999;40(10):2805.